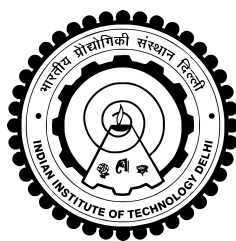


**MORPHOLOGICAL PHASE SEPARATION INDUCED
REGENERATION OF PATTERNS**

ABHISHEK KUMAR BARNWAL



**DEPARTMENT OF CHEMICAL ENGINEERING
INDIAN INSTITUTE OF TECHNOLOGY DELHI**

JULY 2025

**MORPHOLOGICAL PHASE SEPARATION INDUCED
REGENERATION OF PATTERNS**

by

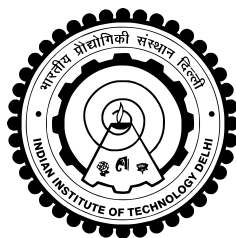
ABHISHEK KUMAR BARNWAL

Department of Chemical Engineering

Submitted

in fulfillment of the requirements of the degree of Doctor of Philosophy

to the



INDIAN INSTITUTE OF TECHNOLOGY DELHI

July 2025

Certificate

This is to certify that the thesis titled “**MORPHOLOGICAL PHASE SEPARATION INDUCED REGENERATION OF PATTERNS**” being submitted by **Mr. Abhishek Kumar Barnwal** in the Department of Chemical Engineering, Indian Institute of Technology, Delhi, for the award of the degree of **Doctor of Philosophy**, is a record of bona-fide research work carried out by him under our guidance and supervision. In our opinion, the thesis has reached the standards fulfilling the requirements of the regulations relating to the degree. The results contained in this thesis have not been submitted for the award of any other degree, diploma, associate-ship or similar title of any university or institution.

Prof. Rajesh Khanna

Professor

Department of Chemical Engineering

Indian Institute of Technology Delhi

Prof. Paresh Chokshi

Professor

Department of Chemical Engineering

Indian Institute of Technology Delhi

Acknowledgments

First and foremost, I am extremely grateful to Prof. Rajesh Khanna, who has been a Guide to me in every possible meaning of the word. I can confidently say that I am both a better researcher and a better individual than I was before I started my Ph.D. and Prof. Khanna is the prominent reason for that.

I am also indebted to co-supervisor Prof. Paresh Chokshi for his insight, suggestions and encouragement. Huge thanks are due to Dr. Avanish Kumar (JNU) for being an excellent collaborator and a friend-in-need during my journey.

I would also like to express my gratitude to my research committee members, Prof. Vivek Vitthal Buwa, Prof. Supreet Singh Bahga and Prof. Mohan Kumar Singh Verma for their valuable suggestions.

I am extremely grateful to all the past and present members of our research group for making the years I spent at the Interfacial and Nanoscience lab the best years of my life. A special thanks to my friends and fellow research scholars at the Department of chemical engineering (IIT Delhi) for the discussions about research that improved my knowledge.

I would also like to thank my dear wife Madhu for her support. Finally, my parents have been a continuous source of inspiration throughout my whole life and I am extremely grateful for their love and encouragement.

Abstract

The thesis presents comprehensive theoretical and numerical investigations of regeneration of physical patterns through morphological phase separation (MPS). A model system of thin liquid films on chemically heterogeneous solid substrates undergoing MPS in a purely apolar force field in the absence of any convection and reaction is chosen to study the regeneration process. The chemical heterogeneities create spatial boundaries to divide the substrate in “source” and “sink” regions separated by a “boundary” region. Sink is the most wettable region, the boundary region is least wettable and the source is region of intermediate wettability. It has been shown previously that unstable thin liquid films on such substrates can form equilibrium patterns in the sink and source regions by redistribution of film liquid through MPS. Liquid flows to the sink from the source by crossing the boundary and fills the sink to its capacity. The spatial boundaries on the substrate localize the liquid in the sink and the source once the sink is “full”. The equilibrium patterns in the source as well as in the sink depend on the volume of liquid in each. The localized liquid in the fully filled sink forms an equilibrium pattern corresponding to the capacity of the sink. The equilibrium pattern in the fully filled sink is “unique” as the capacity of the sink depends on the cross-sectional area of the sink and the equilibrium contact angle of the film liquid on the sink material. This imparts a “Structural” memory to the liquid in the sink. In contrast, the equilibrium pattern in the source is dependent on the amount of left-over liquid which in turn depends on the initial total amount of liquid and capacity of the sink. The equilibrium patterns in the sink are damaged by removing liquid and the regeneration process of the damaged pattern in the sink

is studied based on numerical solution of Thin Film equations. It is shown that the liquid from the source moves preferentially to regenerate the pattern in the sink and can regenerate it completely if there is sufficient liquid in the source region. A new equilibrium pattern is formed in the source corresponding to the remaining amount of liquid in the source. If the liquid in the source is less than what is required for complete regeneration then only partial regeneration is possible and all the liquid in the source is used up. Whenever competing sinks of different chemical nature are present then the regeneration of the pattern in the most wettable sink region is preferred. The sink next in line with respect to wettability is preferred once the pattern in the most wettable sink is regenerated completely. This cascading process of regeneration happens till all the liquid in the source has been used up. The regeneration does not happen in chemically homogeneous substrates in which division of source, sink and boundary is absent. The current study provides a reference point for studying regeneration processes whereby presence of isolated charges, permanent dipoles, convection and reaction is not required for the regeneration. The study will also provide a mechanism for fabrication of self-repairing nanodevices, soft nanomachines, and nanomedicines.

सार

यह शोधप्रबन्ध रूपात्मक चरण पृथक्करण (MPS) के माध्यम से भौतिक प्रतिरूप के पुनरुत्पादन के व्यापक सैद्धांतिक और संख्यात्मक अध्ययनों को प्रस्तुत करती है। पुनरुत्पादन प्रक्रिया का अध्ययन करने के लिए एक नमूना प्रणाली को चुना गया है, जिसमें रासायनिक रूप से विषम ठोस आधार पर पतली तरल परतों का उपयोग किया गया है, जो पूरी तरह से अध्रुवी बल क्षेत्र में, संवहन (convection) और प्रतिक्रिया की अनुपस्थिति में, शोधप्रबन्ध रूपात्मक चरण पृथक्करण (MPS) से गुजरती हैं। रासायनिक विषमताएँ आधार को 'स्रोत' (source) और 'कुण्ड' (sink) क्षेत्रों में विभाजित करने के लिए स्थानिक सीमाएँ बनाती हैं, जो एक 'सीमा' (boundary) क्षेत्र से अलग होती हैं। कुण्ड सबसे अधिक नमनीय क्षेत्र है, सीमा क्षेत्र सबसे कम नमनीय है और स्रोत मध्यवर्ती नमनीयता वाला क्षेत्र है। पहले यह दिखाया गया है कि ऐसे आधार पर अस्थिर पतली तरल परतों शोधप्रबन्ध रूपात्मक चरण पृथक्करण (MPS) के माध्यम से तरल परत के पुनर्वितरण द्वारा 'कुण्ड' (sink) और स्रोत क्षेत्रों में संतुलन प्रतिरूप बना सकती हैं। तरल सीमा को पार करके स्रोत से 'कुण्ड' (sink) में प्रवाहित होता है और 'कुण्ड' (sink) को उसकी क्षमता तक भर देता है। आधार पर स्थानिक सीमाएँ 'कुण्ड' (sink) के 'भर जाने' के बाद 'कुण्ड' (sink) और स्रोत में तरल को स्थानीयकृत करती हैं।

स्रोत के साथ-साथ 'कुण्ड' (sink) में भी संतुलन प्रतिरूप प्रत्येक में तरल की मात्रा पर निर्भर करता है। पूरी तरह से भरे हुए 'कुण्ड' (sink) में स्थानीयकृत तरल 'कुण्ड' (sink) की क्षमता के अनुरूप एक संतुलन प्रतिरूप बनाता है। पूरी तरह से भरे हुए 'कुण्ड' (sink) में संतुलन प्रतिरूप 'अद्वितीय' होता है क्योंकि 'कुण्ड' (sink) की क्षमता 'कुण्ड' (sink) के क्रॉस-सेक्शनल क्षेत्र और 'कुण्ड' (sink) सामग्री पर फिल्म तरल के संतुलन संपर्क कोण पर निर्भर करती है। यह 'कुण्ड' (sink) में तरल को एक 'संरचनात्मक' स्मृति प्रदान करता है। इसके विपरीत, स्रोत में संतुलन प्रतिरूप बचे हुए तरल की मात्रा पर निर्भर करता है, जो बदले में प्रारंभिक कुल तरल मात्रा और 'कुण्ड' (sink) की क्षमता पर निर्भर करता है। 'कुण्ड' (sink) में संतुलन प्रतिरूप को तरल निकालकर क्षतिग्रस्त कर दिया जाता है और पतली फिल्म समीकरणों के संख्यात्मक समाधान के आधार पर 'कुण्ड' (sink) में क्षतिग्रस्त प्रतिरूप की पुनरुत्पादन प्रक्रिया का अध्ययन किया जाता है। यह दिखाया गया है कि स्रोत से तरल 'कुण्ड' (sink) में प्रतिरूप को पुनर्जीवित करने के लिए प्राथमिकता से चलता है और यदि स्रोत क्षेत्र में पर्याप्त तरल है तो इसे पूरी तरह से पुनर्जीवित कर सकता है। स्रोत में बची हुई तरल की मात्रा के अनुरूप एक नया संतुलन प्रतिरूप स्रोत में बनता है। यदि स्रोत में तरल पूर्ण पुनरुत्पादन के लिए आवश्यक से कम है तो केवल आंशिक पुनरुत्पादन संभव है और स्रोत में सभी तरल का उपयोग हो जाता है।

जब विभिन्न रासायनिक प्रकृति के प्रतिस्पर्धी 'कुण्ड' (sink) मौजूद होते हैं, तो सबसे अधिक नमनीय 'कुण्ड' (sink) क्षेत्र में प्रतिरूप का पुनरुत्पादन प्राथमिकता से होता है। एक बार जब सबसे अधिक नमनीय 'कुण्ड' (sink) में प्रतिरूप पूरी तरह से पुनर्जीवित हो जाता है, तो नमनीयता के संबंध में अगले 'कुण्ड' (sink) को प्राथमिकता दी जाती है। पुनरुत्पादन की यह सोपानीकरण प्रक्रिया तब तक होती है जब तक स्रोत में सभी तरल का उपयोग नहीं हो जाता। रासायनिक रूप से सजातीय आधारों में पुनरुत्पादन नहीं होता है जिसमें स्रोत, 'कुण्ड' (sink) और सीमा का विभाजन अनुपस्थित होता है। वर्तमान अध्ययन पुनरुत्पादन प्रक्रियाओं के अध्ययन के लिए एक संदर्भ बिंदु प्रदान करता है जिसमें पुनरुत्पादन के लिए अलग-थलग आवेशों, स्थायी द्विध्रुवों, संवहन और प्रतिक्रिया की उपस्थिति की आवश्यकता नहीं होती है। यह अध्ययन स्व-मरम्मत सूक्ष्मउपकरण, कोमल सूक्ष्मयन्त्र और सूक्ष्मऔषधि के निर्माण के लिए एक तंत्र भी प्रदान करेगा।

Contents

1	INTRODUCTION	1
1.1	Patterns in Nature	1
1.2	Phase Separation in Binary Liquid Mixtures	6
1.3	Morphological Phase Separation and Pattern Formation in Thin Liquid Films	8
1.3.1	Model System of Study	12
1.4	Controlled Pattern Formation in MPS	17
1.5	Self-Healing and Regeneration	18
1.6	Outline and Organization of the Thesis	22
2	MATHEMATICAL MODEL AND NUMERICAL METHOD	25
2.1	Non-Dimensionalization	26
2.2	Numerical Scheme	29
3	SELF HEALING	31
3.1	Localizing Liquid in the Liquid Phase Separation and MPS	36
3.2	Deformation and Healing	38
3.2.1	Source has enough material	39
3.2.2	Not enough material in the source	42
3.3	Summary and Discussions	48
4	PREFERENTIAL SELF-HEALING	53
4.1	Introduction	53

4.2	Methodology	55
4.3	Localizing Material in Phase-Separating Systems: A Pathway to Self- Repairing Nano- structures and Complex Patterns	55
4.4	The Unidirectional Valve Mechanism in Self-Repairing Processes: Lack of Intercommunication Among Distinct Localized Entities	69
4.5	The Unidirectional and Bidirectional Valve Mechanisms in Self-Repair: The Development of Collaborative Interactions Among Distinct Local- ized Entities	71
4.6	Dynamics of Liquid in the Source Region and Equilibrium Responses of Deformed Structures in the Sink	72
4.7	Structural Recovery and Repair Mechanisms	73
5	LOCALIZATION AND DELOCALIZATION	79
5.1	Substrates Divided into Two More and Less Wettable Sub-regions . .	80
5.2	De-localization and Biasing	88
5.3	Summary and Conclusions	92
6	PATTERN FORMATION AND REGENERATION IN NUCLEATED MPS	93
6.1	Pattern Formation in Nucleated MPS	97
6.2	Results and Discussions	102
6.3	Regeneration of Patterns on Homogeneous Substrates	115
6.4	Summary and Conclusion	121
7	CONCLUSIONS	123
	Bibliography	125
	Brief Bio-data of Author	137

List of Figures

- 1.1 Examples of symmetry in nature: A flower displaying the radial symmetry; an underwater scene featuring a coral reef; a close-up view of a honeycomb densely populated with bees; a tiger, whose body stripes exemplify bilateral symmetry common in animals; the cracks of a tree trunk; a snail's spiraled shell demonstrates the elegance of natural spirals and rotational symmetry; a delicate snowflake showcases intricate hexagonal symmetry formed by ice crystals; and a butterfly displays striking bilateral symmetry in its wing patterns. 2
- 1.2 (a) A schematic diagram showing the variation of symmetric free energy, F_m [in arbitrary units] of a binary liquid mixture as given by equation 1.1 with volume fraction of species A , x_A , in the form of a double well at a temperature T . The two finite equilibrium phases are facilitated by Maxwell's common tangent construction (horizontal dotted line). (b) Schematic diagram showing the corresponding phase diagram in terms of T/T_C and x_A obtained from symmetric free energy diagram as shown in the figure (a). T_C is the critical temperature. Unstable, stable and metastable regions in the phase diagram are marked clearly. Note that the phase diagram is also symmetric. 7

1.3	(a) Typical variation of free energy, $\Delta G(h)$ and its double derivative with film thickness h on a solid coated substrate subjected to a long-range attraction and short-range repulsion. (b) Phase diagram in terms of coating thickness and film thickness corresponding to the free energy curves shown in figure (a). The unstable, metastable and stable regions are shown clearly. The diagram has been generated for a thin liquid film system on a coated substrate where the coating provides the short-range repulsion and the underlying solid provides the long-range attraction. The effective Hamaker constants of the film liquid for the substrate and coating are 1.4×10^{-20} and -1.4×10^{-21} , respectively. The free energy curves are shown for coating thickness $128nm$	9
1.4	Various stages of MPS on a uniformly coated substrate in a thin liquid film system. The lateral view is shown in left panels (a–d), the top view of the snapshots of the MPS at non-dimensional time T is shown in right panels (e–h), where H is the non-dimensional film thickness. The system is $(16L_M)^2$ in size. L_M is defined later in equation 2.10. Coating thickness is $192nm$ and initial film thickness is $320nm$. The effective Hamaker constants of the film liquid for the substrate and coating are 1.4×10^{-20} and -1.4×10^{-21} , respectively.	11
1.5	Schematic diagram of the system of thin liquid film on a coated substrate.	13
1.6	A schematic representation of a substrate-coating system using a template based on chemical heterogeneity. Three separate regions—source, sink, and boundary are depicted in the schematic of a typical substrate coating. The surface properties of each region are different, creating heterogeneity on the substrate.	17
1.7	Stable complex 3-D structures created from the MPS of a liquid film, inspired by a star, Fibonacci spiral, sectorized-plate snowflake, glass-hour, honeycomb, a leaf with veins, and structures of varying sizes and shapes [Narayanan et al., 2019 and Kumar et al., 2019]	19

2.1	A schematic diagram of the 3-D thin film system chosen for study. . .	26
2.2	Variation of spinodal parameter or the double derivative of the excess free energy per unit area of the film with respect to film thickness corresponding to equation 2.8.	28
3.1	Schematic diagram: Droplet “A” is ripened and completely localized in a sink. The reference time is $t = t_1$ when we cut the “A”. Droplet “B” represents the damaged droplet after cutting “A”. It is observed that after a time interval Δt , the damaged droplet heals itself with its original shape and size (represented by “C”). The healing time depends on the degree of damage (see fig. 3.4). The healing process also confirms that the structures within the sink are localized structures with a memory.	34
3.2	The left panel and right panel show the free energy, chemical potential and spinodal parameter per unit area vs film thickness plots of source, sink and boundary, respectively. As shown in figure 1.6 for the three different regions. B_{si} and B_{so} are the ratios of the coating and the solid Hamaker constants for the sink and the source, respectively. The boundary’s parameters are different, as the boundary surface energy is opposite to that of the source and sink. The left panel of the diagram is for sink and source, where we can see that the double tangent construction is possible, whereas the right panel represents the boundary. For the boundary, it should be noted that due to the repelling nature, the droplet formation is not possible, and from the right panel of the diagram double tangent construction is not possible, and the behaviour is the opposite of the source and the sink. The above plots are for an aqueous film system with coating thickness $\delta = 196nm$, and the Hamaker constant of the substrate is $A_s = 1.4 \times 10^{-20}$	35
3.3	Phase diagram in terms of coating thickness and film thickness corresponding to the free energy curves.	36

3.4	Cross-sectional heights of a localized droplet at various stages after the cut. Initially, the localized droplet is ripened and is in equilibrium. At this time, the droplet is cut, and subsequently, we observe its growth. After a short time interval, the droplet regains its shape and size. The healing time depends on the degree of healing.	38
3.5	Self-healing of one drop in five liquid drops on the substrate. The lateral view and top view of the snapshots of healing patterns at non-dimensional time T are shown in the left (a-d) and right (e-h) panels, respectively. The results presented are for non-dimensional film thickness H vs time T for the system size $(16L_m)^2$	40
3.6	Self-healing of all drops in five liquid drops on the substrate. The lateral view and top view of the snapshots of healing patterns at non-dimensional time T are shown in the left (a-d) and right (e-h) panels, respectively. The results presented are for non-dimensional film thickness H vs time T for the system size $(16L_m)^2$	41
3.7	Self-healing of a leaf-type complex pattern on the substrate if liquid present in the source. The results presented are for non-dimensional film thickness H vs time T for the system size $(16L_m)^2$	42
3.8	Cross-sectional heights of leaf at various stages. Initially, the leaf pattern is ripened and is in equilibrium. At this time, one leaf is cut, and we observe its growth. After a short time interval, the leaf regains its height. The healing time depends on the degree of healing.	42

3.9 Role of source in healing the damaged structure. In this case, initially we have one localized droplet, and all the extra liquid from the source is removed. The localized droplet is completely cut from its base. We observed that the source tries to repair the damaged droplet. The small amount of liquid provided by the source from the lower thickness maintains the equilibrium of the whole system. However, healing is not possible in this case. We need a larger amount of liquid in the source, or another localized source that can repair the damaged droplet. The lateral view and top view of the snapshots of healing patterns at non-dimensional time T are shown in the left (a-d) and right (e-h) panels, respectively. The results presented are for non-dimensional film thickness H vs time T for the system size $(16L_m)^2$ 44

3.10 Self-healing of a localized liquid drop on the substrate. The lateral view and top view of the snapshots of healing patterns at non-dimensional time T are shown in the left (a-d) and right (e-h) panels, respectively. The results presented are for non-dimensional film thickness H vs time T for the system size $(16L_m)^2$ 45

3.11 Cross-sectional heights of a localized droplet at various stages after the cut. Initially, the localized droplet is ripened and is in equilibrium. At this time, the droplet is cut, and subsequently, we observe its growth. After a short time interval the droplet regains its shape and size. The healing time depends on the degree of healing. 46

3.12 Self-healing of equal wettability drop in two liquid drops on the substrate if limited liquid is present in the source and one drop is damaged. The lateral view and top view of the snapshots of healing patterns at non-dimensional time T are shown in the left (a-d) and right (e-h) panels, respectively. The results presented are for non-dimensional film thickness H vs time T for the system size $(16L_m)^2$ 47

3.13	Cross-sectional heights of two localized droplets at various stages after one drop damaged. Initially, the localized droplet is ripened and is in equilibrium. At this time, one droplet is cut, and we observe its growth. After a short time interval, the droplets attain a new equilibrium height. The healing time depends on the degree of healing.	48
3.14	Self-healing of equal wettability drop in three liquid drops on the substrate if limited liquid is present in the source, and one drop is damaged. The lateral view and top view of the snapshots of healing patterns at non-dimensional time T are shown in the left (a-d) and right (e-h) panels, respectively. The results presented are for non-dimensional film thickness H vs time T for the system size $(16L_m)^2$	49
3.15	Cross-sectional heights of a localized droplet at various stages after one drop damaged and limited liquid present in the source in three equal wettability drop system. Initially, the localized droplet is ripened and is in equilibrium. At this time, the droplet is cut, and subsequently, we observe its growth. After a short time interval, the droplet attains a new equilibrium height. The healing time depends on the degree of healing.	50
4.1	Self-healing of one higher wettability drop in two liquid drops on the substrate if limited liquid is present in the source. The lateral view and top view of the snapshots of the healing patterns at non- dimensional time T are shown in the left (a-d) and right panels (e-h), respectively. The results presented are for non-dimensional film thickness H vs time T for the system size $(16L_m)^2$	58

4.2	Cross-sectional heights of two localized droplets at various stages after higher wettability drop damage. Initially, the localized droplet is ripened and is in equilibrium. At this time, a higher wettability droplet is cut, and subsequently, we observe its growth. After a short time interval, the droplets attain a new equilibrium height. The healing time depends on the degree of healing.	59
4.4	Cross-sectional heights of a localized droplet at various stages after highest wettability drop is damaged. Initially, the localized droplet is ripened and is in equilibrium. At this time, the droplet is cut, and subsequently, we observe its growth. After a short time interval, the droplet regains its shape and size. The healing time depends on the degree of healing.	59
4.3	Self-healing of one of the highest wettability drop in three liquid drops on the substrate if limited liquid is present in the source. The lateral view and top view of the snapshots of the healing patterns at non-dimensional time T are shown in the left (a-d) and right panels (e-h), respectively. The results presented are for non-dimensional film thickness H vs time T for the system size $(16Lm)^2$	60
4.5	Self-healing of medium wettability drop in three liquid drops on the substrate if limited liquid is present in the source. The lateral view and top view of the snapshots of the healing patterns at non-dimensional time T are shown in the left (a-d) and right panel (e-h), respectively. The results presented are for non-dimensional film thickness H vs time T for the system size $(16Lm)^2$	62

4.6	Cross-sectional heights of a localized droplet at various stages after medium wettability drop damaged. Initially, the localized droplet is ripened and is in equilibrium. At this time, the droplet is cut, and subsequently, we observe its growth. After a short time interval, the droplet regains its shape and size. The healing time depends on the degree of healing.	63
4.7	No healing of the lowest wettability drop in three liquid drops on the substrate if limited liquid is present in the source. The lateral view and top view of the snapshots of the healing patterns at non-dimensional time T are shown in the left (a-d) and right panels (e-h), respectively. The results presented are for non-dimensional film thickness H vs time T for the system size $(16Lm)^2$	64
4.8	Cross-sectional heights of a localized droplet at various stages after low wettability drop cut. Initially, the localized droplet is ripened and is in equilibrium. At this time, the droplet is cut, and subsequently, we observe its growth. No recovery.	65
4.9	Self-healing of the lowest wettability drop in three liquid drops on the substrate if extra liquid is inserted in the source. The lateral view and top view of the snapshots of the healing patterns at non-dimensional time T are shown in the left (a-d) and right panel (e-h), respectively. The results presented are for non-dimensional film thickness H vs time T for the system size $(16Lm)^2$	67
4.10	Self-healing of one larger drop in five liquid drops on the substrate. The lateral view and top view of the snapshots of the healing patterns at non-dimensional time T are shown in the left (a-d) and right panels (e-h), respectively. The results presented are for non-dimensional film thickness H vs time T for the system size $(16Lm)^2$	76
5.1	A template of heterogeneous substrate divided into two equal sub-regions.	82

5.2	A typical evolution of a thin film undergoing true MPS on a homogeneous substrate coating thickness $\delta = 192nm$ and film thickness $h_0 = 320nm$. The lateral and top views of the snapshots of the true MPS patterns at non-dimensional time T are shown in the left and right panels, respectively.	83
5.3	Early stage evolution of a thin film undergoing true MPS on a substrate with localization on heterogeneous substrate coating thickness $\delta = 192nm$ and film thickness $h_0 = 320nm$. The lateral and top views of the snapshots of the true MPS patterns at non-dimensional time T are shown in the left and right panels, respectively.	84
5.4	Late stage evolution of a thin film undergoing phase separation on a substrate with localization on $\delta = 192nm$ and $h_0 = 320nm$. The lateral view and top view of the snapshots of localized patterns at non-dimensional time T are shown in the left and right panels, respectively.	85
5.5	Early stage evolution of a thin film undergoing phase separation on a substrate with de-localization on heterogeneous substrate coating thickness $\delta = 192nm$ and film thickness $h_0 = 320nm$. The lateral and top views of the snapshots of de-localized patterns at non-dimensional time T are shown in the left and right panels, respectively.	86
5.6	Late stage evolution of a thin film undergoing true MPS on a substrate with delocalization on $\delta = 192nm$ and $h_0 = 320nm$. The lateral view and top view of the snapshots of de-localized patterns at non-dimensional time T are shown in the left and right panels, respectively.	87
5.7	Early stage evolution of a thin film undergoing true MPS on a substrate with de-localization on $\delta = 192nm$ and $h_0 = 350nm$. The lateral and top views of the snapshots of de-localized patterns at non-dimensional time T are shown in the left and right panels, respectively.	89

5.8	Late stage evolution of a thin film undergoing true MPS on a substrate with de-localization on $\delta = 192nm$ and $h_0 = 350nm$. The lateral view and top view of the snapshots of de-localized patterns at non-dimensional time T are shown in the left and right panels, respectively.	90
5.9	A typical evolution of a thin film undergoing true MPS on a substrate with de-localization on $\delta = 192nm$ and $h_0 = 370nm$. The lateral and top views of the snapshots of de-localized patterns at non-dimensional time T are shown in the left and right panels, respectively.	91
5.10	Normalized entropy of spontaneous MPS, Localization and de-localization.	92
6.1	Phase diagram of the thin film system of homogeneous wettable coating on non-wettable solid substrate. Stable, unstable and metastable regions can be seen, marked by the binodal and spinodal curves. The crosses in the phase diagram show the midpoints of the pair of coexisting thicknesses, marked by filled circles and as defined by the lever rule. The midpoints are marked by hm_i where i is the corresponding coating thickness in nm. Note that because of the asymmetry, the midpoint shifts to more right and lead to metastable regions. The system parameters are $A_s = 1.4 \times 10^{-20}$ and $A_c = -1.4 \times 10^{-21}$	94
6.2	Morphological evolution of nucleation-initiated phase separation on coating thickness $192nm$ and film thickness $409nm$. The lateral view and top view of the snapshots of the nucleated patterns at non-dimensional time T are shown in the left and right panels, respectively.	105
6.3	Plot showing the height of the film along the diagonal corresponding to Fig. 6.5. In the late stages, holes grow by filling the smaller holes. This behaviour is different from the conventional hole growth in the deep inside the spinodal regime (DISR) where small holes merge into bigger holes and the dynamics proceeds through diffusion in the late stages.	106

6.4	Morphological evolution of nucleation-initiated phase separation on coating thickness $112nm$ and film thickness $467nm$. The lateral and top views of the snapshots of the true MPS patterns at non-dimensional time T are shown in the left and right panels, respectively.	107
6.5	Early stage Pattern formation during true MPS of a $487nm$ homogeneous film on $112nm$ coating which lies close to the spinodal boundary. The lateral view and top view of the snapshots of the true MPS patterns at non-dimensional time T are shown in the left and right panels, respectively.	108
6.6	Late stage Pattern formation during true MPS of a $487nm$ homogeneous film on $112nm$ coating, which lies close to the spinodal boundary. The lateral view and top view of the snapshots of the true MPS patterns at non-dimensional time T are shown in the left and right panels, respectively.	109
6.7	Pattern formation during true MPS of a $510nm$ homogeneous film on $112nm$ coating which lies close to the spinodal boundary. The lateral and top views of the snapshots of the true MPS patterns at non-dimensional time T are shown in the left and right panels, respectively.	111
6.8	Plot showing the height of the film along the diagonal for Fig. 6.7. In the late stages, we observe that the hole of a bigger radius grows by breaking the boundary between the smaller holes, which are connected. This behaviour is opposite to that shown in Fig. 6.3. The expansion of a bigger hole continues until a single hole with a large ridge or plateau is obtained. This picture is not conventional in DISR. The dynamics of pattern formation follows different routes in different scenario of nucleation and growth.	112

6.9	Pattern formation during true MPS of a $533nm$ homogeneous film on $96nm$ coating which lies close to the spinodal boundary. The lateral and top views of the snapshots of the true MPS patterns at non-dimensional time T are shown in the left and right panels, respectively.	113
6.10	Morphological evolution of nucleation-initiated phase separation on coating thickness $128nm$ and film thickness $387nm$. The lateral view and top view of the snapshots of the nucleated patterns at non-dimensional time T are shown in the left and right panels, respectively.	116
6.11	Failure to self-heal in droplets if parts of the system are damaged on homogeneous substrate ($\delta = 96 \text{ nm}, h_0 = 533 \text{ nm}$) with MPS. The lateral view and top view of the snapshots of the healing process by morphological phase separation at non-dimensional time T are shown in panels (a-c) and (d-f), respectively.	118
6.12	failure to self-heal in droplet if parts of the system are damaged on homogeneous substrate ($\delta = 192 \text{ nm}, h = 320 \text{ nm}$) with nucleation. The lateral view and top view of the snapshots of the healing process by morphological phase separation at non-dimensional time T are shown in panels (a-c) and (d-f), respectively.	119
6.13	Self-healing of droplet if parts of the system are damaged on homogeneous substrate ($\delta = 128 \text{ nm}, h = 427 \text{ nm}$) with nucleation. The lateral view and top view of the snapshots of the healing process by morphological phase separation at non-dimensional time T are shown in panels (a-c) and (d-f), respectively.	120